Pulse shaping in strong-field ionization: Theory and experiments

Shuai Li, Bethany Jochim, Jacob Stamm, Dian Peng, Hua-Chieh Shao, Jean Marcel Ngoko Djiokap, and Marcos Dantus

Phys. Rev. A **105**, 053105 — Published 6 May 2022

DOI: 10.1103/PhysRevA.105.053105

Pulse shaping in strong-field ionization: theory and experiments

Shuai Li,[1] Bethany Jochim,[1] Jacob Stamm,[1] Dian Peng,[2] Hua-Chieh Shao,[2] Jean Marcel Ngoko Djiokap,[2] and Marcos Dantus[1,3]*

[1] *Department of Chemistry, Michigan State University, East Lansing, MI 48824, USA*

[2] *Department of Physics and Astronomy, University of Nebraska, Lincoln, Nebraska 68588, USA*

[3] *Department of Physics and Astronomy, Michigan State University, East Lansing, MI 48824, USA*

Intense ultrafast pulses cause dissociative ionization and shaping the pulses may allow control of both electronic and nuclear dynamics that determine ion yields. We report on a combined experimental and theoretical effort to determine how shaped laser pulses affect tunnel ionization, the process that precedes many strong-field phenomena. We carried out experiments on Ar, N_2, H_2O, and O_2 using a phase step function of amplitude $¾\pi$ that is scanned across the spectrum of the pulse. In addition, we changed the amount of chirp in the pulses. Semiclassical as well as fully quantum mechanical time-dependent Schrödinger equation calculations are found to be in excellent agreement with experimental results. We find that precise knowledge of the field parameters in the time and frequency domains is essential to afford reproducible results and quantitative theory and experiment comparisons.

I. INTRODUCTION

Intense laser fields cause molecules to ionize and fragment. The yield of different product ions from this interaction depends on the temporal profile of femtosecond laser pulses [1]. These early observations led to a large body of research on the use of shaped laser pulses to control the fragmentation of many different molecules, a body of work that has been summarized elsewhere [2,3]. The recent observation of order-of-magnitude changes in the non-sequential double ionization (NSDI) of methanol and ethane molecules by shaped laser pulses [4,5] inspired this scientific collaboration to find a satisfying physical explanation for the observed phenomenon. We seek to understand why a spectral phase step with amplitude of $¾\pi$ was found to enhance or suppress NSDI, depending on if it is positively or negatively detuned in position from the carrier frequency of the pulse. Our presentation focuses on the strong-field ionization (SFI) process that precedes fragmentation and/or NSDI and how it is affected by a single-phase step that is scanned across the spectrum of intense femtosecond pulses.

When an atom or molecule absorbs more photons than the minimum needed for ionization, above-threshold ionization occurs [6,7]. As the field strength and wavelength increase, tunnel ionization, rather than multiphoton ionization, dominates. The Keldysh parameter, γ, helps determine which ionization regime is dominant [8]. Given $\gamma = \omega_0\sqrt{2I_p}/F_0$, where ω_0 is the central angular frequency of the laser, I_p is the ionization potential, and F_0 the field strength, when $\gamma > 1$ (weaker pulses and shorter wavelengths) the ionization process is considered to be multiphoton, and for $\gamma < 1$ (stronger pulses and longer wavelengths) the ionization takes place via tunneling. During tunnel ionization the intense laser field distorts the binding potential, resulting in tunnel ionization; the free electron wave packet may then be accelerated by the laser field. Finally, the laser field switches direction, returning the electron wave packet back to the parent ion with much greater energy, such that it may lead to NSDI as well as high-harmonic generation (HHG). Tunnel ionization is integral to the three-step model [9,10], which is used to explain HHG driven by optical fields. In the tunnel ionization process, the field strength impacts the rate of ionization and the energy of the electrons, but the wavelength of the laser also plays a decisive role. The ponderomotive energy, U_p, is the cycle-averaged kinetic energy gained by a free electron in a laser field F_0 and is expressed in eV as

$$U_p = \frac{F_0^2}{4\omega_0^2} \approx 9.3\times10^{-5} I\lambda^2 \qquad (1)$$

where I is the laser intensity in petawatts per cm^2 and λ is the wavelength in nm. As can be seen

from the above expression, longer wavelengths lead to higher electron kinetic energies.

We focus on using a spectral phase step to explore its effect on SFI. The use of a phase step for controlling multiphoton processes has a rich history. The initial work by Meshulach and Silberberg [11,12], focused on coherent quantum control (CQC) of two-photon transitions in caesium atoms. They explained the observed control using perturbation theory to calculate the second-order power spectrum (SOPS) of the shaped laser pulses and showed that the overlap between the two-photon cross section of the atom and the SOPS determines the transition probability. It seemed from the early work that CQC would not work on large molecules, especially those in solution [12]. Dantus and coworkers, extended the CQC approach to control the two- and three-photon transitions of large molecules in solution, [13, 14], an approach that became useful for biomedical imaging [15,16,17]. CQC has more recently been used to enhance stimulated emission and to control the virtual and dipole pathway contributions to two-photon transitions in large molecules in solution [18,19].

Extension of the CQC approach to strong-field control of two-photon transitions in atomic sodium atoms by Trallero and co-workers [20] showed that as the laser intensity increases, dynamic Stark shifts and ground-state depletion cause the frequency-domain explanation for CQC to break down. Similar effects were found by Suchowski et al., where the symmetry resulting from the SOPS breaks down by power broadening and Stark shifts [21]. In the intermediate intensity regime, Amitay and co-workers observed the emergence of four-photon transitions in sodium atoms [22]. The experiments described so far can be adequately modelled using perturbation theory, up to the point that the predicted resonances are washed out.

In this paper, a joint experimental and theoretical study is carried out to demonstrate how shaped laser pulses significantly affect tunnel ionization of argon and atmospheric molecules. The pulse shaping is performed by scanning a phase step function across the spectrum of a reference pulse, while manipulating the amount of chirp in the pulses. Such pulse shaping leads to dramatic changes in the pulse intensity that are reflected in the ion yields, as well as in other related observables such as the relative difference and ratio. The observed effects are very different from what would be predicted from perturbation theory. In section II, we provide key details about our experiments. In section III, a basic parameterization of the shaped pulse is presented, and we describe the theoretical treatment of SFI by semiclassical and quantum mechanical formalisms. In Section IV, we then present experimental results on atomic and diatomic systems and compare our results with those obtained by theory. Finally, we provide analysis of the shaped laser fields that reveals how interference caused by a step function of amplitude $a\pi$ (a is a non-integer) shifted away from ω_0 can introduce a chirp on the pulses.

II. EXPERIMENTAL DETAILS

The ionization yields from Ar and the molecular targets are measured using a Wiley-McLaren time-of-flight (TOF) spectrometer [23]. The ion signals from a microchannel plate detector are digitized by a fast oscilloscope, allowing determination of the relative yields. Our spectrometer includes a 1-mm-wide slit in the extraction electrode serving to reduce focal-volume-averaging effects [24]. The Ar gas is introduced into the TOF chamber via a needle valve, whereas the highlighted molecular ions H_2O^+, N_2^+, and O_2^+ arise from ionization of background gas in the chamber. In this way, we measure all the ions simultaneously. The pressure in the chamber was in the mid-10^{-7}-Torr range during the measurements.

The linearly polarized laser pulses used were generated by a titanium sapphire chirped pulse amplification laser system at a repetition rate of 1 kHz and with a central wavelength of about 790 nm. The pulses were characterized and compressed via the multiphoton intrapulse interference scan (MIIPS) method using a MIIPS-HD pulse shaper [25]. Second and third order dispersion were minimized further by scanning $\pi/2$ phase-step scans while recording the second-harmonic spectrum of the pulses [26]. The Fourier transform-limited (TL) pulses had a full-width at half maximum (FWHM) duration of 36 fs. The pulse shaper was then utilized to precisely apply various combinations of chirp and phase steps to these pulses. The pulses are focused by a 300-mm focal length lens into the TOF chamber to a peak intensity of 2×10^{14} W/cm^2, which was estimated by evaluating the Ar^{2+}/Ar^+ ratio [27].

These parameters lead to γ of about 0.8 for Ar and N_2 and about 0.7 for H_2O and O_2.

III. THEORY

Calculations are performed based on the tunnel ionization formula [28,29] and by solving the time-dependent Schrödinger equation (TDSE) within the single active electron (SAE) approximation. We restrict our simulations to Ar atoms for simplicity. Because this ionization process takes place in the strong-field regime, such numerical simulations for Ar atoms provide a good account for the general mechanism of ionization of N_2 molecules (with a very similar binding energy) and the other molecular species.

A. The Shaped Field

Addressing the effect of pulse shaping on tunnel ionization requires a rigorous definition of the shaped pulses, as well as precise experimental control of the laser field as described later. The laser pulses, prior to pulse shaping, are given by

$$I_{TL}(t) = \exp\left[-g^2(t/\tau_f)^2\right]. \quad (2)$$

Here, I_{TL} is the time-dependent intensity, τ_f is the pulse duration (FWHM in intensity), and $g = 2\sqrt{\ln 2}$.

Pulse shaping is best accomplished in the frequency domain using a programmable pulse shaper [30]. Therefore, we define the field in the frequency domain assuming Gaussian pulses:

$$\tilde{F}(\omega) \equiv \sqrt{S(\omega)}e^{i\varphi(\omega)}, \quad (3)$$

where

$$S(\omega) = \exp\left[-g^2(\omega-\omega_0)^2/\sigma_f^2\right] \quad (4)$$

is the spectrum of the pulse, with a bandwidth σ_f FWHM and centered at ω_0. The pulse duration is related to its bandwidth by the time-bandwidth product $\sigma_f\tau_f \geq g^2$, with equality indicating TL pulses. The spectral phase $\varphi(\omega)$ is given by

$$\varphi(\omega) = \frac{\beta_2}{2!}(\omega-\omega_0)^2 + \frac{\beta_3}{3!}(\omega-\omega_0)^3 + \ldots, \quad (5)$$

where β_2 and β_3 are the second- and third-order dispersion terms. The time-dependent description of the field is thus obtained by Fourier transformation:

$$F(t) \equiv \frac{1}{2\pi}\int_{-\infty}^{+\infty}\sqrt{S(\omega)}\, e^{i\varphi(\omega)}e^{-i\omega t}\, d\omega\,. \quad (6)$$

In addition to dispersion, we introduce a phase-step of amplitude ¾π, such that the phase equals zero until the phase-step position where it acquires a value of +¾π or −¾π. The phase step has a signficant effect on the pulse in the time domain. When the phase step is located at ω_0, the pulse is broken into two closely spaced pulses in the time domain without further dispersion. When the phase step is detuned from the center frequency, the pulse acquires a dispersive effect that switches sign between the two pulses.

B. Semiclassical Simulation

The ionization probability of a single Ar atom from its ground state is obtained by integrating the ionization rate over the duration of the laser field:

$$P(t_f) = \int_{t_0}^{t_f} G(t)W(t)\,dt\,. \quad (7)$$

The laser field runs from time t_0 to t_f, and we choose a time interval long enough such that the ionization is not sensitive to the pulse duration. $G(t)$ is the ground state population at time t: $G(t) \approx 1 - P(t)$. The adiabatic approximation [29] is considered, meaning that for a time-varying laser field $F(t)$, ionization happens as if within a static field at time t. The ionization rate $\mathrm{W}[F(t)]$ is calculated using the rate for a system bound by a short-range potential W_{SR} with a Coulomb correction Q:

$$\mathrm{W}(F) = Q(F)W_{\mathrm{SR}}(F), \quad (8)$$

where W_{SR} is given as Eq. (54) of Ref. [29] without a cycle-average factor $\sqrt{3F/(\pi\kappa^3)}$ and Q is given in Eq. (5) of Ref. [31]. The final form of $W(F)$ is

$$W(F) = I_p C_{\kappa l}^2 \frac{(2l+1)(l+|m|)!}{2^{|m|}|m|!(l-|m|)!}(1+\gamma^2)^{|m|/2+3/4}\left(1+\frac{2\gamma}{e}\right)^{-2Z/\kappa} A_m(\omega,\gamma)\times \left(\frac{2\kappa^3}{F}\right)^{2Z/\kappa-|m|-1}\exp\left[-\frac{2\kappa^3}{3F}g(\gamma)\right], \quad (9)$$

where atomic units (a.u.) are used and $F = |F(t)|$, I_p is the ionization potential, γ is the Keldysh parameter, $\kappa = \sqrt{2I_p}$, and $Z = 1$ is the charge of atomic residue after ionization. $g(\gamma)$ is given in Eq. (33) of Ref. [29]. $A_m(\omega,\gamma)$ describes a sum of many-photon processes and is given in Eq. (55) of Ref. [29]. We set the angular momentum $l = 1$, magnetic quantum number $m = 0$, and $C_{\kappa 1} = 2.13$ [28]. Note that we calculate ionization rates using electric fields $F(t)$ with the carrier frequency, because a cycle-average factor is not included in Eq. (9) (this factor is given in, e.g., Eq. (7) of Ref. [29]). If this cycle-average factor is included, one should use the temporal envelope of the pulse [32].

The ionization yield of Ar is then obtained by averaging a Gaussian intensity profile in the cross section of a propagating laser pulse at the focus:

$$\mathrm{Y} = \int_0^{h_{\max}} 2\pi h P(h)\,dh\,, \quad (10)$$

where P is calculated using Eq. (7) and $h_{\max}$ is set to be the beam waist. For the field, we use parameters that closely match the experimental pulses. Specifically, we used TL Gaussian pulses with a carrier wavelength of 799.4 nm, a pulse duration of 37 fs and a peak intensity of 2×10^{14} W/cm^2 (0.0755 a.u.). We then introduced the phase step as described above.

C. Quantum Mechanical Simulation

Given that the Keldysh parameter varies with the intensity of the laser pulse, from below one to above one during the laser pulse, we find that the semiclassical Ammosov-Delone-Krainov (ADK) formula [28] is not sufficient to provide a complete understanding of the ionization processes. For this reason, we adopt a quantum mechanical approach by solving the TDSE within the electric dipole approximation, in which the spatial dependence of the electric field and the magnetic field are neglected. To calculate the Ar ionization yield and other observables such as the relative difference and related ratio for the step at position $\omega-\omega_0$ in rad/fs and chirp in fs^2, we solve the TDSE within the SAE approximation by neglecting electron-electron correlations.

The numerical methods for solving the TDSE for the laser-atom system are described elsewhere [33,34], so we only summarize here. The TDSE for the laser-atom system is

$$\partial_t \Psi(\vec{r},t) = \left[H_0 + V(t)\right]\Psi(\vec{r},t), \quad (11)$$

where H_0 is the field-free Hamiltonian of the Ar atom; and $V(t) = -\vec{d}\cdot\vec{F}(t)$ describes the laser-atom interaction, with $\vec{d}$ being the dipole operator, and $\vec{F}(t)$ being the electric field. The field-free Hamiltonian involves the kinetic energy operator of the active election and an atomic potential. For the Ar atom, we employ a model potential [35] to correctly calculate the energies of the field-free ground state and ionization potential. The atomic potential has the form of

$$V_{at}(r) = -\frac{Z_c + a_1 e^{-a_2 r} + a_3 e^{-a_4 r} + a_5 e^{-a_6 r}}{r} \quad (12)$$

where Z_c is the asymptotic charge of the active electron, and a_j $(j = 1-6)$ are the parameters obtained by fitting the numerical potential calculated from self-interaction free density functional theory and fine-tuned such that the ionization potential matches experiments. For numerical values of Z_c and a_j for Ar atoms, see Ref. [35]. This model potential has been shown to be valid from the regime of tunnelling ionization to barrier-suppression ionization where the ADK formula fails. The sharp phase jump introduced in the laser spectrum causes long temporal tails whose duration extends over 1 ps. This long duration is challenging for a time-dependent simulation. However, we found that the dominant ionization

comes from the part of the laser profile with greater amplitude. Therefore, a window function $e^{-(t/\tau)^{10}}$ is employed to reduce the long laser profile. The window width τ is chosen to be large enough such that the ionization yield is not sensitive to its variation. Our simulations use $\tau = 643$ fs.

The wave function $\Psi(\vec{r},t)$ is expanded in spherical harmonics $Y_{\ell m}(\hat{r})$, while its coefficient radial part $u_{\ell m}(\hat{r},t)$ is propagated in time on a radial-angular momentum grid using the Crank-Nicolson and split-operator schemes. To discretize the radial part $u_{\ell m}(\hat{r},t)$ of the wave function, we use a square root radial grid whose mesh points are denser close to the origin to account for the rapid oscillation of the wave function near the core. The kinetic energy operator in the field-free Hamiltonian is approximated by a three-point finite difference. An absorption boundary is used at radius $r = 300$ a.u. to absorb the outgoing wave function of the ionized electron. For the $3p_0$ ground state of Ar considered here, the initial condition for $u_{\ell m}(\hat{r},t)$ is given by the angular momentum $\ell = 1$ and the magnetic quantum number $m = 0$. Because the laser pulse is linearly polarized, $[H_0, L_z] = 0$ and the magnetic quantum number m is conserved, meaning that it remains equal to its initial quantum value $m = 0$ during the time propagation. After the laser pulse, the ionization yield is calculated using the probability that the active electron remains bound. All simulations have been tested for convergence with a numerical accuracy on the order of a few percent.

IV. RESULTS & DISCUSSION

As mentioned, the experiments reported here are for an atomic target (Ar) and three molecular species (N_2, H_2O, and O_2) whose binding energies are 15.759 eV, 15.581 eV, 12.621 eV, and 12.070 eV, respectively [36].

For the first experiments, the pulses were shaped by a phase step located at a point that is positively or negatively detuned from ω_0 by 0.025 rad/fs. For each case, we calculated the relative difference (RD), defined as

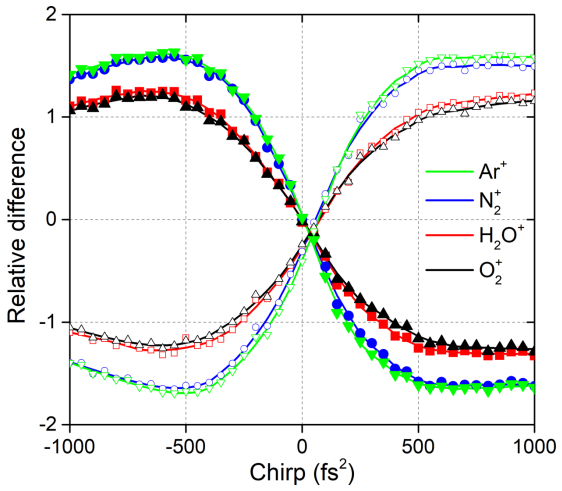

Fig. 1. Experimentally measured relative difference of the ion yields obtained as a function of scanning the chirp of pulses with a step at +0.025 rad/fs (filled symbols) or -0.025 rad/fs (open symbols).

$$RD = \frac{Y_+ - Y_-}{(Y_+ + Y_-)/2}, \qquad (13)$$

where Y_+ and Y_- indicate the ionization yield in the case where the phase step has a positive or negative amplitude, respectively. The measurements, shown in Fig. 1, were repeated as a function of chirp value, which was scanned from -1000 to 1000 fs^2. We observe that the relative difference is essentially zero in the absence of chirp. The slight deviation from zero is caused by uncorrected chirp of about 35 fs^2 which causes a pulse broadening of about 0.1 fs. This level of residual chirp is very difficult to measure and correct, especially in situ. When the phase step is detuned by +0.025 rad/fs, the relative difference is positive for negative chirp and negative for positive chirp, a result that is qualitatively similar for the four ionic species being compared. We also find that the result is reversed when the phase step is detuned by −0.025 rad/fs. Larger differences are found for Ar and N_2 and smaller differences for O_2 and H_2O. These differences are due to the ionization potentials of the targets. When $Y_+ = 10Y_-$, RD equals 1.64. The results shown in Fig. 1 indicate that the phase step is causing a chirp in the shaped field. This concept is explored later.

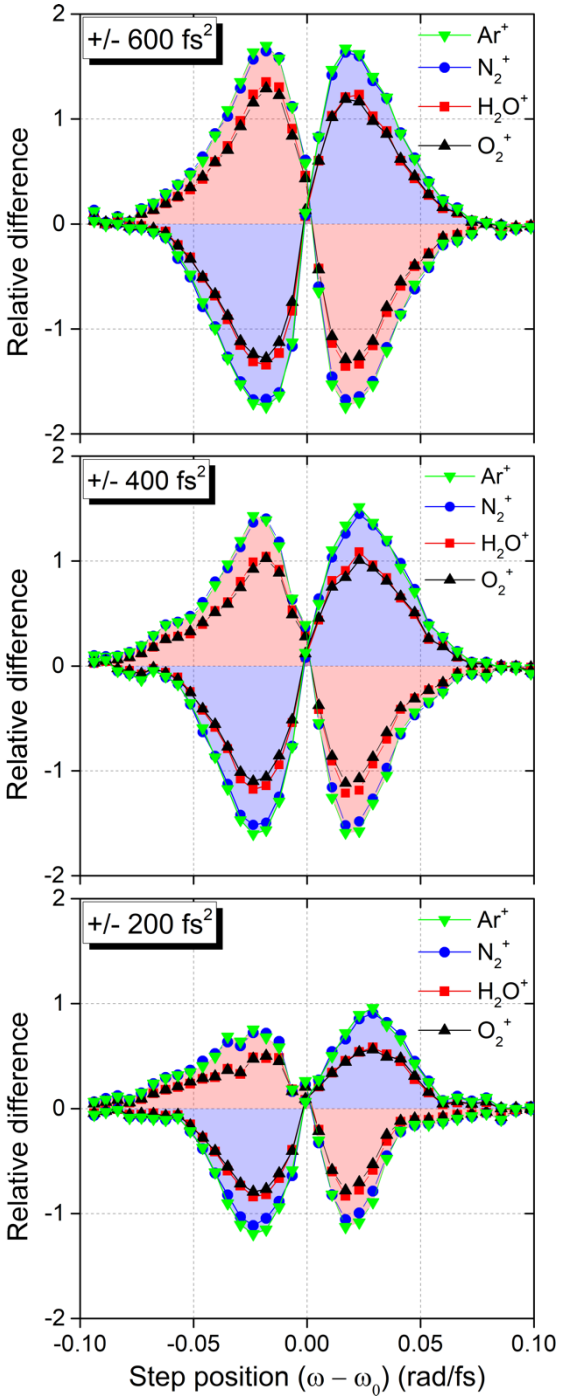

Fig. 2. Experimentally measured relative difference, defined by Eq. (13), of the ion yields obtained as a function of position of the phase step for a given positive (pink shading under curve) or negative (blue shading under curve) chirp value indicated in each plot.

The next sets of experiments, shown in Fig. 2, were obtained for a fixed amount of chirp, and the position of the step was scanned from −0.1 to 0.1 rad/fs with respect to ω_0. These scans were

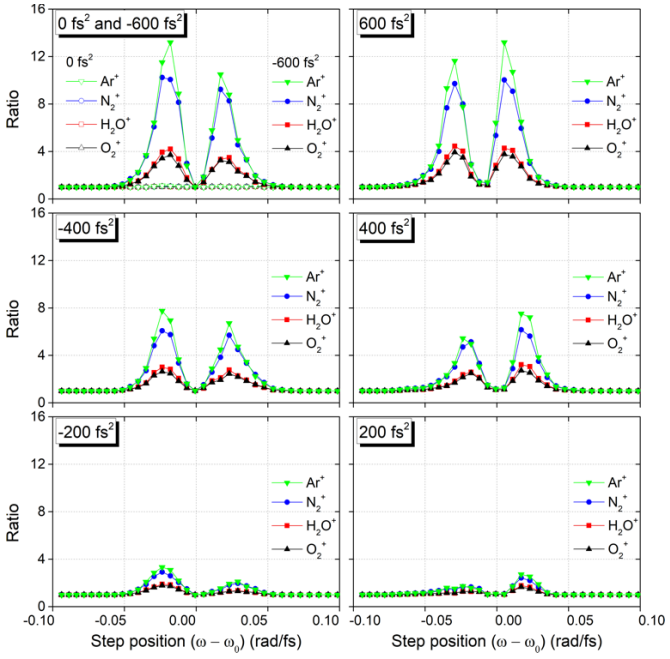

Fig. 3. Experimentally measured ratios Y_+/Y_- or Y_-/Y_+ of the ion yields obtained as a function of scanning the position of the phase step for a given positive or negative chirp value indicated in each plot. The nominator and denominator are chosen so that values are always greater than one.

repeated for positive (pink shading under curve) and negative (blue shading under curve) chirp values ranging from 0 to 600 fs^2. Again, the relative difference is defined according to Eq. (13). When comparing the three panels in Fig. 2 from the top to the bottom, one observes that the magnitude of the relative difference is greatest for ±600 fs^2 and decreases as one approaches zero chirp. This is consistent with the observations in Fig. 1.

We find it instructive to also plot the data shown in Fig. 2 in terms of the ratio of the yields obtained Y_+/Y_- or Y_-/Y_+ depending on which ratio results in values greater than one. These results, plotted in Fig. 3, illustrate the magnitude of the obtained tunnel ionization yields, which exceed an order of magnitude for a set of added chirp values ranging from +600 to −600 fs^2. We observe the maximum ratio, >12, for the largest chirp value and that the ratio is approximately one in the absence of chirp. We also note that ion yield ratios are not symmetric about step position ω_0. This is because the pulse strength is not symmetric. For example, when the pulse chirp is +600 fs^2, the peak-intensity ratio (positive/negative step) at step position −0.025 rad/fs is 1.64 and the peak-intensity ratio

(negative/positive) at step position +0.025 rad/fs is 1.67. Therefore, the ion-yield ratio is larger for a positive detuning of the phase step.

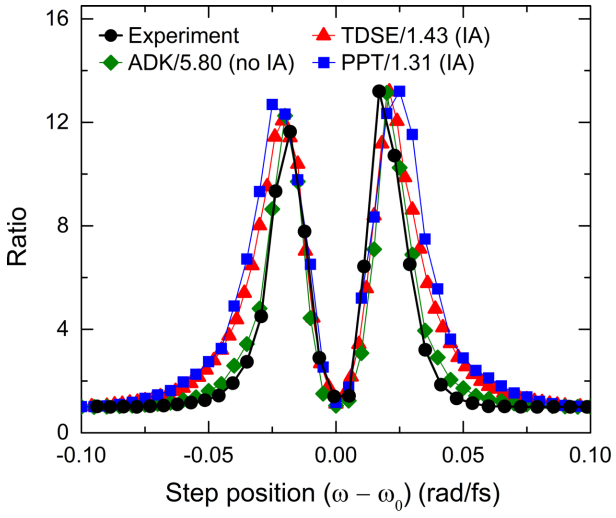

Fig. 4. Results of simulations and TDSE calculations for Ar atoms. We performed intensity averaging for each curve labeled "IA." The chirp value is +600 fs^2. The simulations and calculations are scaled to match the right peak in the experimental data, which is shown for comparison.

Results from the analytic as well as the quantum mechanical calculations are shown in Fig. 4 in terms of the ratio between the ion yields for positive and negative phase steps. Each result from the PPT (obtained from Section III. B) and TDSE calculations displayed in Fig. 4 are obtained by intensity averaging according to Eq. (10). These intensity averaging calculations are based on calculations for about 20 values of the pulse peak intensity. As a reference, the Keldysh parameter corresponding to pulse intensities at the focus, i.e., h=0 in Eq. (10), ranges from 0.94 to 1.37. Clearly, we find very good agreement between the two theoretical approaches, as well as with experimental results. The theoretical results from ADK formula [28] without intensity averaging are also displayed in Fig. 4. One sees that ADK results (valid for Keldysh parameters much less than one) overestimate the ratio by a factor of about 6. Strikingly, the asymmetry exhibited by the ratio experimentally is well reproduced by each of the three theoretical approaches.

In Fig. 5 we plot TL and shaped pulses with a ¾ step at ω_0 or detuned by −0.03 rad/fs from ω_0. We show both Wigner and Husimi time-frequency representations to illustrate the amplitude and phase of the shaped pulses. The expression for the Wigner representation is given by

$$W(\tilde{F};t,\omega)=\int_{-\infty}^{\infty}\tilde{F}(\omega+\Omega)\tilde{F}(\omega-\Omega)^{*}e^{i2\Omega t}\,d\Omega, \qquad (14)$$

where $\tilde{F}(\omega)$ is taken from eq. (3). The Husimi distribution is obtained by two-dimensional convolution of the Wigner represenation with a bandwidth-limited Gaussian pulse whose duration equals that of the TL pulses. We find that the change in phase by the step causes destructive interference in portions of the pulse, and the presence of the abrupt change causes the pulse to broaden. (see Fig. 5). When the phase step is negatively detuned from ω_0, we observe an up-chirp followed by a down-chirp in the high-intensity portion of the pulse. This behavior has not been identified in previous coherent control work involving phase-step shaped pulses because a π-phase step does not cause a chirp. The chirp appears for steps of amplitudes that are non-integer multiples of π.

In a recent publication by the Dantus group, π/2-phase step shaped pulses were found to be uniquely sensitive to chirp and third-order dispersion (TOD) in femtosecond laser pulses [26]. In that study, the second harmonic of the shaped pulses was detected as a function of step position. The contour map resulting from the difference of data obtained using positive and negative phase steps revealed features that could be quantitatively reduced to the amount of chirp and TOD on the input pulses. When the input pulses had no dispersion, then no features are observed in the difference contour map. Once the dispersion was measured, it could be corrected until phase distortions were reduced down to a few milliradians within the FWHM of the pulses. In contrast to that work, when determining the relative difference (see Eq. (13)) we find the greatest contrast when the amplitude of the step is ¾π.

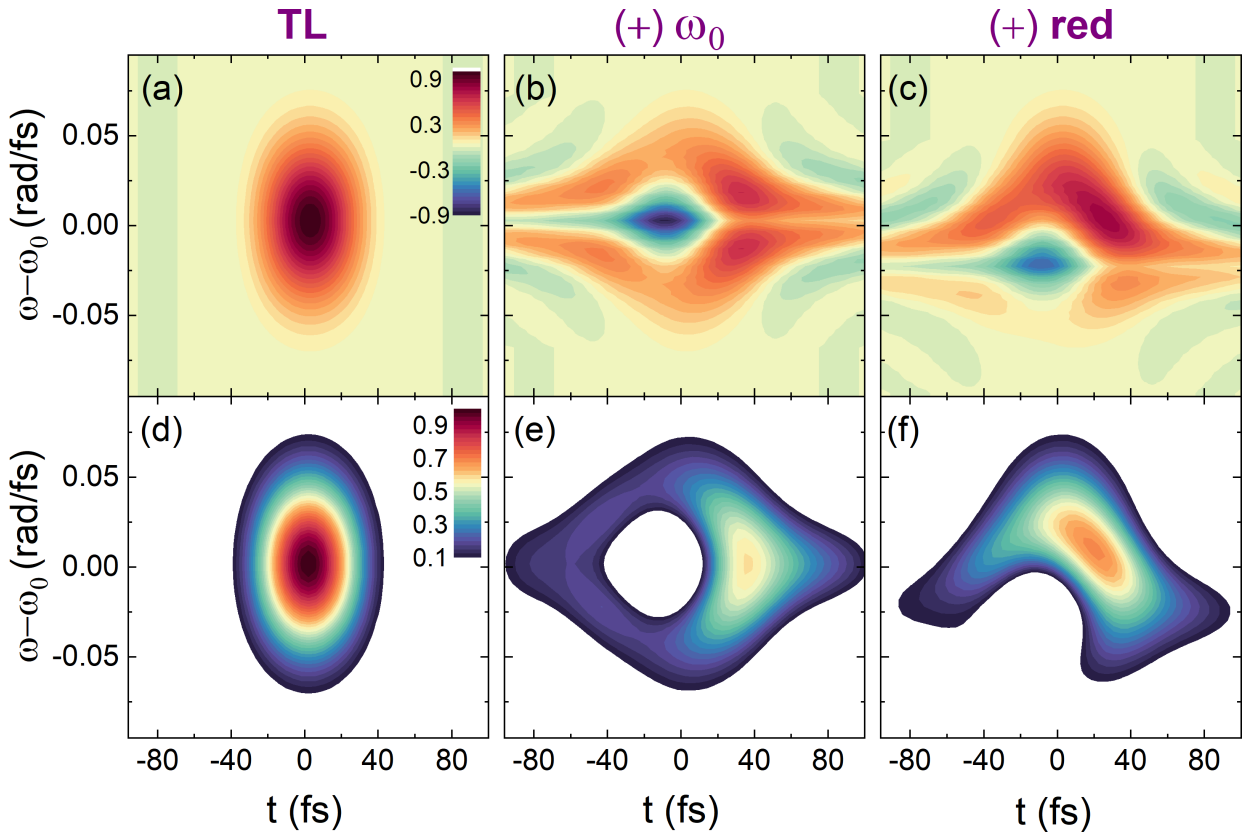

Fig. 5. Time-frequency Wigner (top) and Husimi (bottom) representations of 40-fs TL, pulses shaped with a ¾ π step at ω_0, and at ω_0−0.03 rad/fs. The plots are calculated using Eq. (14).

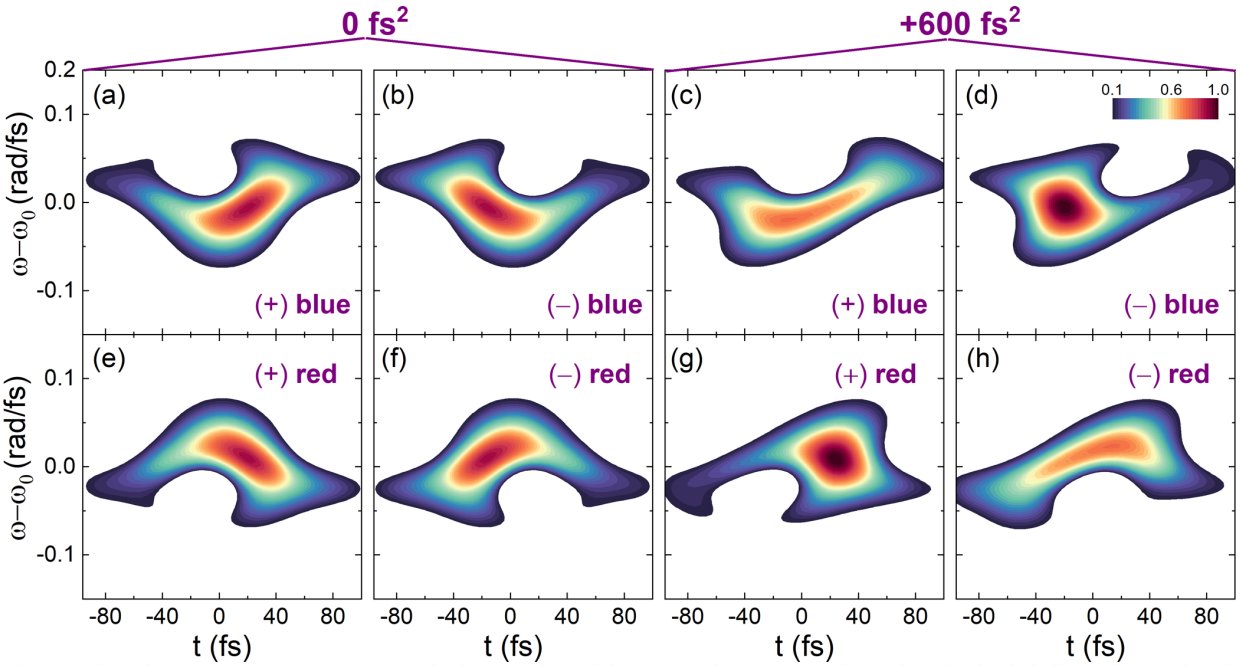

Fig. 6. Time-frequency representations of a laser pulse with a ±¾π phase step. The pulses in the left four plots (a,b,e,f) have zero chirp in addition to the phase step, whereas those in the right plots (c,d,g,h) have +600 fs^2 chirp. The "blue" plots indicate a positive detuning of the step position from the central frequency to +0.03 rad/fs, and the "red" ones indicate a negative detuning to −0.03 rad/fs. Furthermore, the "(+)" labels indicate a +¾π spectral phase step, and "(−)" labels indicate a −¾π step. The plots are calculated using Eq. (14).

The chirp introduced by a phase step of amplitude $a\pi$, where a is a non-integer, detuned from the center frequency, reduces the peak intensity of the pulses. In Fig. 6(left), we show the Husimi representaton of pulses that are shaped by a $\pm\frac{3}{4}\pi$ phase step and are positively or negatively detuned. The sign of the chirp and the sign of the detuning play similar roles, and this results in the relative symmetry between the sign of the chirp and the sign of the phase step that was observed when studying the NSDI process in ethane using phase step shaped pules [4]. Compensating for the chirp introduced by the phase step and recovering the pulse peak intensity requires the introduction of a pre-chirp with the opposite sign. When we introduce a chirp of +600 fs^2, we find that two of the pulses regain intensity close to their TL value, but the other two become even broader and weaker. When considering strong-field laser matter interactions, which are higly nonlinear in nature, the effects described here are greatly amplified.

The key observation is that due to the dispersive effect of the phase step, the more intense portion of the pulse can acquire an up-chirp, see [Fig. 6 (a) and (f)] or down-chirp [Fig. 6 (b) and (e)]. When the dispersive effect of the phase step is counteracted by chirp, as in panels (d) and (g), the pulse regains its intensity, and when the dispersion is increased by chirp, the pulse decreases in intensity as in panels (c) and (h).

V. CONCLUSIONS

The goal of this joint experimental and theoretical work was to explain the order-of-magnitude changes in the NSDI of methanol and ethane molecules by shaped laser pulses [4,5]. A review of previous work on the use of phase steps for controlling nonlinear optical processes in weak and stronger fields did not provide a satisfactory explanation. Experimental results following the SFI of Ar, N_2, O_2, and H_2O with a combination of a positive or negative $\frac{3}{4}p$ phase step detuned from the carrier frequency, with the addition of chirp, reproduced the changes in ion yield and symmetry that had been observed in [4,5]. Semiclassical and quantum mechanical simulations for strong-field interactions with Ar atoms using the experimental laser parameters were carried out. Upon intensity averaging, we find very good agreement between the quantum mechanical TDSE calculations and analytic calculations based upon an improved PPT formula for the ionization rate (which spans the range of the Keldysh parameter from multiphoton to tunnel ionization). Moreover, those theoretical calculations are found to be in quantitative agreement with the experimental results.

A Wigner and Husimi time and frequency description of the pulses was used to reveal how a phase step of with a non-integer multiple of π amplitude that is detuned from the carrier frequency of the pulse, introduces up- and down-chirps on the laser pulse. The lobe with the highest intensity being the one that determines the outcome of strong-field interactions receiving a chirp whose sign depends on the sign of the phase step and its position, i.e., detuned to higher or lower frequencies. The dependence on step sign and detuning, leads to the experimentally observed symmetry.

The experimental results and theory presented here help understand the effect of pulse shaping using phase step functions on strong-field induced tunnel ionization. Specifically, we find that phase steps in the frequency domain with non-integer multiple of π amplitude and detuned from the carrier frequency can introduce chirps in the laser pulse. The chirp imparted on the most intense part of the pulse affects tunnel ionization. The addition of chirp by the pulse shaper or by dispersive optics can amplify or mitigate the chirp induced by the phase step function. It is reasonable to assume that the understanding gained here in terms of tunnel ionization can be extended to several different phenomena that stem from tunnel ionization, such as NSDI, ATI, HHG, and others.

We find that the magnitude and sign of the chirp needed to affect strong-field measurements is well below what can be measured by conventional pulse characterization methods, especially as the measurement needs to be carried out in situ. This has important implications for reproducibility of pulse shaping in strong-field experiments. Scanning a $\frac{3}{4}\pi$ phase step is therefore a very sensitive approach to determine in situ if the pulses being used in strong-field measurements are transform limited or if they have a small

residual chirp. Finally, it is worth highlighting the excellent agreement between calculations and experiments for the systematic pulse shaping approach used here, a level of agreement not often found in strong field work.

VI. AKNOWLEDGMENTS

This material is based upon work supported by the U.S. Department of Energy, Office of Science, Office of Basic Energy Sciences, Atomic, Molecular and Optical Sciences Program under Award Number SISGR (DE-SC0002325). The theoretical work at the University of Nebraska was supported in part by the US National Science Foundation under Grant No. PHYS-1505492 [D.P., H.C.S. and J.M.N.D.] and by the U.S. Department of Energy (DOE), Office of Science, Basic Energy Sciences, under Award No. DE-SC0021054 [J.M.N.D]. Our TDSE calculations were completed utilizing the Holland Computing Center of the University of Nebraska, which receives support from the Nebraska Research Initiative.

[1] A. Assion, T. Baumert, M. Bergt, T. Brixner, B. Kiefer, V. Sayfried, M. Strehle, G. Gerber, *Science* **282**, 919 (1998).
[2] V. V. Lozovoy, X. Zhu, T. C. Gunaratne, D. A. Harris, J. C. Shane, M. Dantus, *J. Phys. Chem. A* **112**, 3789 (2008).
[3] V. V. Lozovoy, M. Dantus, *Annu. Rep. Prog. Chem., Sect. C: Phys. Chem.,* **102**, 227 (2006).
[4] S. Li, D. Sierra-Costa, M. J. Michie, I. Ben-Itzhak, M. Dantus, *Commun. Phys.* **3**, 35 (2020).
[5] M. J. Michie, N. Ekanayake, N. P. Weingartz, J. Stamm, M. Dantus, *J. Chem. Phys.* **150**, 044303 (2019).
[6] P. Agostini, F. Fabre, G. Mainfray, G. Petite, N. K. Rahman, *Phys. Rev. Lett.* **42**, 1127 (1979).
[7] K. J. Schafer, B. Yang, L. F. DiMauro, K. C. Kulander, *Phys. Rev. Lett.* **70**, 1599 (1993).
[8] L. V. Keldysh, *Sov. Phys. JETP* **20**, 1307 (1965).
[9] P. B. Corkum, *Phys. Rev. Lett.* **71**, 1994 (1993).
[10] K. C. Kulander, K. J. Schafer, J. L. Krause, "Dynamics of Short-Pulse Excitation, Ionization and Harmonic Conversion," in *Super-Intense Laser-Atom Physics*, B. Piraux, A. L'Huillier, K. Rzążewski, Eds., 95−110 (1993).
[11] D. Meshulach, Y. Silberberg, *Nature* **396**, 239 (1998).
[12] D. Meshulach, Y. Silberberg, *Phys. Rev. A* **60**, 1287 (1999).
[13] K. A. Walowicz, I. Pastirk, V. V. Lozovoy, M. Dantus, *J. Phys. Chem. A* **106**, 9369 (2002).
[14] V. V. Lozovoy, I. Pastirk, K. A. Walowicz, M. Dantus, *J. Chem. Phys.* **118**, 3187 (2003).
[15] I. Pastirk, J. M. Dela Cruz, K. A. Walowicz, V. V. Lozovoy, M. Dantus, *Opt. Express* **11**, 1695 (2003).
[16] J. M. Dela Cruz, I. Pastirk, M. Comstock, V. V. Lozovoy, M. Dantus, *Proc. Nat. Acad. Sci.* USA **101**, 16996 (2004).
[17] H. Tu, Y. Liu, D. Turchinovich, M. Marjanovic, J.K. Lyngsø, et al., *Nat. Photonics* **10**, 534 (2016).
[18] A. Konar, V. V Lozovoy, M. Dantus, *J. Phys. Chem. A* **120**, 2002 (2016).
[19] J. Lahiri, S. H. Yuwono, I. Magoulas, M. Moemeni, B. Borhan, G. J. Blanchard, P. Piecuch, M. Dantus, *J. Phys. Chem. A* **125**, 7534 (2021).
[20] C. Trallero-Herrero, T. C. Weinacht, *Phys. Rev. A* **75**, 063401 (2007).
[21] H. Suchowski, A. Natan, B. D. Bruner, Y. Silberberg, *J. Phys. B: At. Mol. Opt. Phys.* **41**, 074008 (2008).
[22] L. Chuntonov, L. Rybak, A. Gandman, Z. Amitay, *Phys. Rev. A* **77**, 021403(R) (2008).
[23] W. C. Wiley and I. H. McLaren, *Rev. Sci. Inst.* **26**, 1150 (1955)
[24] S. M. Hankin, D. M. Villeneuve, P. B. Corkum, D. M. Rayner *Phys. Rev. A* **64**, 013405 (2001).
[25] V. V. Lozovoy, I. Pastirk, M. Dantus, *Opt. Lett.* **29**, 775 (2004).
[26] J. Stamm, J. Benel, E. Escoto, G. Steinmeyer, M. Dantus, *Opt. Express* **29**, 14314 (2021).
[27] C. Guo, M. Li, J. P. Nibarger, G. N. Gibson, *Phys. Rev. A* **58**, R4271 (1998).
[28] M. V. Ammosov, N. B. Delone, V. Kraĭnov, *Zh. Eksp. Teor. Fiz.* **91**, 2008 (1986).
[29] A. M. Perelomov, V.S. Popov, M.V. Terent'ev, *Sov. Phys. JETP* **23**, 924 (1966).
[30] A. M. Weiner, *Opt. Comm.* **284**, 3669 (2011).
[31] S. V. Popruzhenko, V. D. Mur, V. S. Popov, D. Bauer, *Phys. Rev. Lett.* **101**, 193003 (2008).
[32] S.-F. Zhao, A.-T. Le, C. Jin, X. Wang, C. D. Lin, *Phys. Rev. A* **93**, 023413 (2016).
[33] F. Robicheaux, *J. Phys. B* **45**, 135007 (2012).
[34] H.-C. Shao and F. Robicheaux, *Phys. Rev. A* **93**, 053414 (2016).
[35] X. M. Tong and C. D. Lin *J. Phys. B.* **38** 2593 (2005).
[36] NIST Chemistry WebBook, https://webbook.nist.gov/